

Received October 19, 2021, accepted November 24, 2021, date of publication December 13, 2021, date of current version January 7, 2022.

Digital Object Identifier 10.1109/ACCESS.2021.3135382

# Millimetre-Wave Propagation Channel Based on NYUSIM Channel Model With Consideration of Rain Fade in Tropical Climates

ASMA ALI BUDALAL<sup>1,2</sup>, IBRAHEEM SHAYEA<sup>3</sup>,  
MD. RAFIQL ISLAM<sup>2</sup>, (Senior Member, IEEE), MARWAN HADRI AZMI<sup>4</sup>,  
HAFIZAL MOHAMAD<sup>5</sup>, (Senior Member, IEEE), SAWSAN ALI SAAD<sup>6</sup>,  
AND YOUSEF IBRAHIM DARADKEH<sup>7</sup>

<sup>1</sup>College of Electrical and Electronics Technology–Benghazi, Benghazi, Libya

<sup>2</sup>Department of Electrical and Computer Engineering, International Islamic University Malaysia (IIUM), Kuala Lumpur 53100, Malaysia

<sup>3</sup>Department of Electronics and Communication Engineering, Faculty of Electrical and Electronics Engineering, Istanbul Technical University (ITU), 34467 Istanbul, Turkey

<sup>4</sup>Wireless Communication Centre, School of Electrical Engineering, Faculty of Engineering, Universiti Teknologi Malaysia (UTM), Johor Bahru 81310, Malaysia

<sup>5</sup>Faculty of Engineering and Built Environment, Universiti Sains Islam Malaysia, Bandar Baru Nilai, Nilai 71800, Malaysia

<sup>6</sup>Department of Computer Engineering, College of Computer Science and Engineering, University of Ha'il, Ha'il 55211, Saudi Arabia

<sup>7</sup>College of Engineering at Wadi Addawasir, Prince Sattam Bin Abdulaziz University, Al Kharj 11991, Saudi Arabia

Corresponding author: Asma Ali Budalal (asma.budalal@gmail.com)

This work was supported in part by the Ministry of Higher Education Malaysia (MOHE) through the Fundamental Research Grant Scheme under Grant FRGS/1/2019/TK04/UTM/02/34; in part by Universiti Teknologi Malaysia (UTM) through the Collaborative Research Grant (CRG) under Grant R.J130000.7351.4B468; in part by the Higher Institution Centre of Excellence (HICOE) under Grant R.J130000.7851.4J413 and Grant R.J130000.7851.4J493; and in part by the Universiti Sains Islam Malaysia (USIM), Malaysia.

**ABSTRACT** The impact of atmospheric attenuation on wireless communication links is much more severe and complicated in tropical regions. That is due to the extreme temperatures, intense humidity, foliage and higher precipitation rain rates with large raindrop sizes. This paper investigates the propagation of the mm-waves at the 38 GHz link based on real measurement data collected from outdoor microcellular systems in Malaysia. The rainfall rate and received signal level have been measured simultaneously in 1-minute time intervals for one year over a 300 m path length. The rain attenuation distributions at different percentages of exceedance time have been compared with the modified distance factor of the ITU-R P.530-17 model. The average link availability calculated with the measured rain rates has been analysed. Additionally, the key propagation channel parameters such as the path loss, path loss exponent, Rician K-factor, root mean square, delay spread and received power have been investigated considering the rain attenuation. These propagation channel parameters have been analysed using MATLAB software and explained with the help of the latest NYUSIM channel model software package (Version 2.0). The analysis results have been classified considering rain attenuation, antenna setup, link distances, antenna height and antenna gain. The outcomes revealed that the rain fade predicted by applying the modified distance factor provides high consistency with the measured fade in Malaysia and several available measurements from different locations. The large-scale path loss model in the NYUSIM simulation result was around 126.23 dB by considering the rain attenuation effects on the 300m path length. This work shows that the NYUSIM channel model offers more accurate rendering results of path loss for omnidirectional and directional antenna transmissions without rain fade. This study proves that the ability to provide good coverage and ultra-reliable communication for outdoor and outdoor-to-indoor applications during rain in tropical regions must be sufficiently addressed.

**INDEX TERMS** Millimetre-wave, propagation channel, large-scale parameters, distance factor of the ITU-R P.530-17 model, NYUSIM channel model, rain fade, tropical regions.

## I. INTRODUCTION

The use of high millimetre-wave (mm-wave) bands for future outdoor and indoor cellular systems has gained much

The associate editor coordinating the review of this manuscript and approving it for publication was Franco Fuschini<sup>1</sup>.

interest in recent years. Although the implementation of the mm-wave adds several issues to existing networks [1]–[5], it has become a major technological enabler for fifth-generation (5G) and sixth-generation (6G) cellular Technologies. More mm-wave band spectrums are now available, allowing the allocation of more bandwidths in new

communication systems. This significantly contributes to higher download speed, lower latency and more device connections to each cell [6]. It has been proposed that the design of the next-generation mobile communication systems should be supported by optimising system capacity to meet quality and ultra-reliable communications criteria. The literature has also reported that the terrestrial link quality at mm-wave undergoes extreme propagation issues. In addition, weather factors affect signal attenuation, such as rain and humidity. These factors should be extensively considered in the evaluation of wireless link performance and channel modelling. The propagation status, fading characteristics and rain attenuation represent significant challenges for mm-wave links in tropical climates. Since each country's environment and topography differs, an accurate 5G channel model should be developed to identify the optimal performance of specific areas. Deploying mm-wave frequency-based 5G mobile networks in a particular environment will require the propagation characteristics of that environment.

The major challenge is the unavailability of any standard channel model that properly works throughout all deployment scenarios within various environments. Employing channel simulators and computer-aided design tools plays a crucial role in cost-effectively representing and producing the propagation channel behaviour. The reliability of the physical layer design is significantly affected by the propagation channel model. This will consequently reflect on the outage probability, signal to bit error rate (BER), interference plus noise ratio (SINR), symbol error rate (SER) and packet error rate (PER). Channel impairments can be considerably affected by weather conditions and different atmospheric attenuation factors [7], [8]. After acquiring adequate measurements, numerous wideband channel models that signify the impact of 'temporal' and 'spatial' features have been proposed for higher frequency bands [9], [10]. However, a comprehensive understanding of mm-wave propagation and channel characterisation is still needed, especially for higher frequency bands influenced by rain attenuation due to the received signals absorption, scattering, and short-term fluctuation. The propagation channel at mm-wave frequencies must be fully characterised.

Recent outdoor measurements have confirmed that carrier frequencies at 28 GHz and 38 GHz will give optimal performance and work more effectively in specific areas at a small cell size in the 200 m [11], [12]. Researchers have emphasised that rain-induced attenuation can be avoided for mm-wave bands with a small cell coverage area. Links in outdoor environments can be attained by employing optimum antenna configurations such as beam tracking, beam-steering, array antennas, intelligent beamforming techniques and high-gain horn antennas. This is necessary to overcome high-frequency channel impairments and severe path loss [13]–[15]. In contrast, other 5G propagation channel research involving tropical climate regions have highlighted that rain-induced attenuation should not be neglected. Further investigations of link-level performance indicators are necessary to determine

whether a small cell size having a radius of 200 m offers complete coverage for new short-distance mm-Wave systems in tropical climates [4], [18]–[22].

The authors of [16] acquired measurements at 60-GHz frequency band to investigate the large-scale parameters (LSP) and small-scale parameters (SSP) of several propagation channels, such as the multipath channel, path loss and shadow fading, the root-mean-square (RMS) delay spread. In [17], channel estimation at 32 GHz was accomplished for the outdoor microcells scenario. The quasi-deterministic radio channel generator (QuaDRiGa) platform prescribed by 3GPP [18] was used to complete the channel simulation and extract LSPs. The simulated and measured results of LSPs were then compared. Although it was designed for channel simulations below 6 GHz, the authors concluded that the QuaDRiGa is a good platform for the mm-wave band. However, several studies have developed different antenna setups, path loss, shadow fading (SF), Rician distribution with factor  $K$  and RMS, delay spread for mm-wave channel characteristics under the impact of rain fading.

Several previous studies had focused on rain attenuation analysis and modelling. Some considered the received signal strength under different meteorological parameters and the probability of network failure due to rain attenuation and excessive mm-wave loss [8], [19]. Line-of-sight (LOS) and non-line-of-sight (NLOS) scenarios for outdoor measurements have been applied for different frequency bands to assess channel propagation features in tropical regions [20], [21]. The time dispersion parameters and path loss properties were modelled when transmitting 5G signals over a significantly short path.

A comprehensive literature review on mm-wave propagation shows that accurate propagation models become critical, necessitating, for designing new mm-Wave signalling protocols [22]. Even though many candidate frequencies have been examined, only a few measurements in outdoor microcellular systems have been conducted at 38 GHz 5G and sixth-generation 6G cellular network technologies. Particularly in the tropical areas that experience a high probability of convective rainfall with large drop sizes compared to temperate regions worldwide [18]. However, previous works took measurements at short distances (from 10 m to 50 m) during clear skies or very short periods. These studies were primarily based on measurement data collected at specific geographical areas, making them unsuitable to be implemented in other environments. Channel modelling is unavailable at some frequency bands and channel sounding systems, especially during tropical precipitation. Several studies were based in temperate areas with lower rain intensities [8], [23]–[36]. Therefore, research on rain fade and propagation measurements remain insufficient.

This paper analyses the impact of rain on 38 GHz LOS mm-wave transmission link with 0.3 km path length based on actual measurement data. The study aims to characterise and assess the mm-wave channel during different meteorological conditions. The one-minute rain rate integration time and

received signal strength have been processed and examined using MATLAB software. Further assessments have been made for the number of events per year and the probability of rain attenuation occurrences for different measured attenuation levels. The impact of rain-induced attenuation on the mm-wave link availability has also been investigated.

The NYUSIM simulator has been employed to explore the effectiveness of the proposed channel model simulator and characterise the impact of rain attenuation on large-scale parameters of the mm-wave propagation channel in tropical climates.

The NYUSIM simulator was first developed by researchers at New York University based on extensive measurements of candidate spectrum bands for 5G. In the NYUSIM channel model, rain attenuation has been added to all time-varying envelopes of multipath components of the received signal in the channel impulse response (CIR). Comprehensive simulation results are valuable for designing future mobile broadband for outdoor applications. The brief key contributions of this work can be summarised and listed in points as in the following:

- This study has investigated the propagation of mm-waves link at 38 GHz link based on real measurement data collected from outdoor (UMi) systems in Malaysia. The system measured the rainfall rate and received signal level simultaneously in 1-min time intervals for one year over a 300 m path length with a typical line-of-sight (LOS) link. In addition, we investigated the empirical cumulative distribution function (CDF) of the maximum rain attenuation at the experimental 38 GHz link at different % of the time.
- In this work, the results of the rain attenuation in Malaysia and previous studies conducted in different regions compared them with the modified distance factor of the well-known prediction models (ITU-R P. 530-17) for different frequencies over a short path length. The goal is to guarantee reliable mm-wave links, regardless of the undesired effects of meteorological conditions and rain fade phenomena. Thus, a link availability and fade margin estimated with the measured rain rates has been analysed.
- Also, this study investigated the effect of rain attenuation on large-scale mm-wave channel propagation characteristics by utilising MATLAB software with an mm-wave channel simulator NYUSIM software package (Version 2.0). The key propagation channel parameters, such as the path loss, path loss exponent, Rician K-factor, root mean square, delay spread, and received power considering the rain attenuation was studied. The analysis results have been classified considering rain attenuation, antenna setup, link distances, antenna height and antenna gain.
- These results can be used for a large-scale channel model in link budgets to estimate: transmitted power, antenna gains and the number of antenna elements required for beamforming technic, receiver characteristics (e.g., noise figure), and link distance, determine the coverage area

by considering rain attenuation characteristics in tropical regions like Malaysia. The measurements also contribute to the body of knowledge on wireless channel propagation path loss for bands near 38 GHz.

This article is organised as follows: Section II presents the statistical spatial channel model (SSCM). Section III highlights the parameter estimation for channel modelling. Sections IV examines the rain rate and rain attenuation measurements. Section V displays the power delay profile while considering the weather conditions of Kuala Lumpur. Section VI describes the fundamental parameter analysis and channel characterisation. Finally, Section VII presents the conclusion of this work.

## II. STATISTICAL SPATIAL CHANNEL MODEL

The SSCM was developed by NYU WIRELESS. A validated standardised channel model has been considered. It is one of the stochastic spatial channel models classified under the physical millimetre-wave outdoor channel modelling approach. From 2012 to 2019, NYU WIRELESS acquired mm-wave measurements for several outdoor settings in rural macrocell (RMa), urban macrocell (UMa) and urban microcell (UMi) environments with different frequencies and operating scenarios that ranged from 28 to 73 GHz [11], [12], [37]–[43]. They developed simple, uncomplicated models that require less time. NYU WIRELESS also provided the actual performance of CIRs in a similar space and time. NYUSIM fits a wide range of operating frequencies, ranging from 500 MHz to 100 GHz bands, with RF bandwidths between 0 to 800 MHz. It incorporates multi-antenna systems, antenna beamwidths and Multiple-Input Multiple-Output (MIMO) antenna arrays. It further considers atmospheric attenuation issues induced by rain, vapour, haze/fog, dry air (containing oxygen) and foliage in path loss modelling. For their models, NYU WIRELESS used the NYUSIM software package, Version 1.6, created on December 15th, 2017 [44]. The current NYUSIM software package (Version 2.0) uses MATLAB code to generate various channel parameters. Human blockage, spatial consistency and outdoor-to-indoor (O2I) penetration loss (considered a significant channel modelling component) are all implemented in NYUSIM 2.0 [45].

## III. PARAMETERS FOR CHANNEL ESTIMATION

Various channel parameters directly impact the system performance of channel characterisations based on different operating scenarios and environmental conditions [16]. (LSP) generally identify the critical parameters for the path loss (PL), RMS delay spread, shadow fading (SF), azimuth spread (AS) and Rician K-factor. The cross-correlation of large-scale parameters improves link and system-level simulations' spatial consistency and accuracy [43]. It reflects the channel fading features for critical applications that possess stringent reliability requirements. The propagation channel's multipath component, which presents (SSP), will cause the received signal level to fluctuate around its mean value. SSP,

therefore, plays a pivotal role in the design of the physical layer [46]. Hence, this paper investigates the essential LSP required for implementing the NYUSIM model while considering the impact of antenna type, height, gain, operating frequency, mm-wave link length and climatic rain conditions in tropical climates due to higher precipitation rates.

### A. POWER DELAY PROFILE

Due to propagation time delays, the power delay profile (PDP) gives the received signal intensity over different multipath channels [12] as a function of time delay. It is utilised to provide the RMS delay spread and determine the number of multipath components above the noise threshold due to the associated delays [47]. PDP also provides an accurate physical description of the first arriving (shortest delay) multipath component in LOS environments to determine path loss effects when 5G signals spread over mm-wave channels.

### B. PATH LOSS (PL)

Path loss is an essential input parameter in all channel modelling of wireless communication. It is used to illustrate the communication channel between TX-RX. It considers the TX-RX separation distances, distinct scenarios, transmission environment and operating frequency [46]. PL further indicates the average received signal power relative to the transmit power. It is calculated as a function of propagation distance and is a significant factor for link budget, system coverage and interference analysis. It is also a critical parameter in computing the (SINR) of a cellular system [48]. The work in [46] focused on a comprehensive survey to predict wireless network coverage based on path loss models. A higher path loss characterises the mm-wave channel. Thus, the coverage will be restricted to roughly 200 m, making it the most appropriate for its application in indoor hotspots and small outdoor cell scenarios [47]. Different empirical path loss models have been proposed and categorised based on pertinent factors such as terrain, operating frequency range, terrain and mobile generation standards. The most popular models developed to dictate the RF cell size for the mm-wave band include the Stanford University Interim (SUI) alpha-beta-gamma (ABG), close-in (CI) and the floating-intercept (FI) models [12], [46], [48].

It is noteworthy that the (CI) PL model has better stability and accuracy and is less complex. The channel is simulated using NYUSIM, where the close-in model is utilised to develop the omnidirectional and directional path loss models. Additional attenuation and channel variations due to various types of weather factors have been explored in the NYUSIM channel model and are expressed as follows:

$$PL(f, d)[dB] = FSPL(f, d_0)[dB] + 10n\log_{10}\left(\frac{d}{d_0}\right) + AT[dB] + \chi_{\sigma}CI \quad (1)$$

$$FSPL [dB] = 32.4 [dB] + 20\log_{10}(f) + 20\log(d) \quad (2)$$

where  $FSPL(f, d_0)$  [dB] indicates the signal strength at an exact distance in free space at the carrier frequency ( $f$ ),

$n$  is the path loss exponent (PLE), where  $d_0$  is set to 1 m in the NYUSIM channel model [49],  $d$  is the T-R separation distance in meters where  $d \geq d_0$ ,  $\chi_{\sigma}CI$  is the zero-mean Gaussian random variable with a standard deviation  $\sigma$  in dB which models large-scale signal fluctuations and  $AT$  is the atmospheric attenuation given by:

$$AT[dB] = \alpha[dB/m] \times d[m]. \quad (3)$$

Here,  $\alpha$  is the attenuation factor in dB/m for the frequency range of 1 GHz to 100 GHz caused by atmospheric gases, fog, rain, snow and haze [44], [45]. The path loss exponent  $n$  is calculated as follows:

$$n = \frac{R_s - \alpha[dB/m] \times d[m] - \chi_{\sigma}CI}{10\log_{10}(d)} \quad (4)$$

where  $R_s$  is the average received signal measured and  $\alpha$  is the attenuation.

$$\chi_{\sigma}CI = PL^{CI}(f, d) [dB] - FSPL(f, d_0) [dB] - 10n\log_{10}(d) - AT [dB] \quad (5)$$

It is crucial to determine the functional coverage area of base stations in tropical regions and assess the outage probability to enable mobile broadband outdoor applications using mm-wave links. This paper has conducted day and night measurements to investigate the impact of rain-induced attenuation at 38 GHz on the outdoor path loss model.

### C. DESIRED POWER AT THE RECEIVER

Analytical estimation of the desired power for a point-to-point LOS mm-wave link at the receiver antenna has been conducted using Friis's formula [49] given by:

$$P_{R_x,u} [dBm] = P_{T_x} [dBm] + G_{T_x}a [dBi] + G_{R_x}a [dBi] - FSPL(f, d) [dB] \quad (6)$$

The unfaded received signal level,  $P_{R_x,u}$ , is specified by the ( $FSPL$ ), the transmitted power ( $P_{T_x}$ ) and the antenna gain. As shown in Figure 1, the maximum permitted attenuation is called the fade margin (FM), which should recompense for all undesirable factors corrupting the mm-wave link availability: atmospheric attenuation phenomena rain, fog, dust, snow, diffraction and interference. On the other hand, if attenuation exceeds the link margin, the reliability of the physical layer will be affected strongly, and the link will fail and suffers an outage. Therefore, link design must depend on propagation properties, rainfall statistics and knowledge of multipath conditions to estimate radio link length and achieve high percentage availability [54]. The (FM) is the difference between the unfaded received signal level and the receiver sensitivity threshold given by:

$$FM [dB] = P_{R_x,u} [dBm] - P_{R_x,th} [dBm] \quad (7)$$

The summary of notation and parameters of equations are illustrated in Table 1.

TABLE 1. Summary of notation and parameters of equations.

Notation	Definitions
$P_{Rx}$ [dBm]	The desired power at the receive
$P_{Tx}$ [dBm]	The transmit power
$G_{TXa}$	Transmitting antenna gain
$G_{RXa}$	Receiver antenna gain
PL	The propagation loss
FSPL [dB]	The loss of free space
Ar	Attenuation due to rain
Ao	Obstacle loss
Aa	Attenuation due to atmospheric gases
FM [dB]	Fade margin
$P_{Rxu}$ [dBm]	The unfaded received signal level
$P_{Rxth}$	Receiver sensitivity threshold

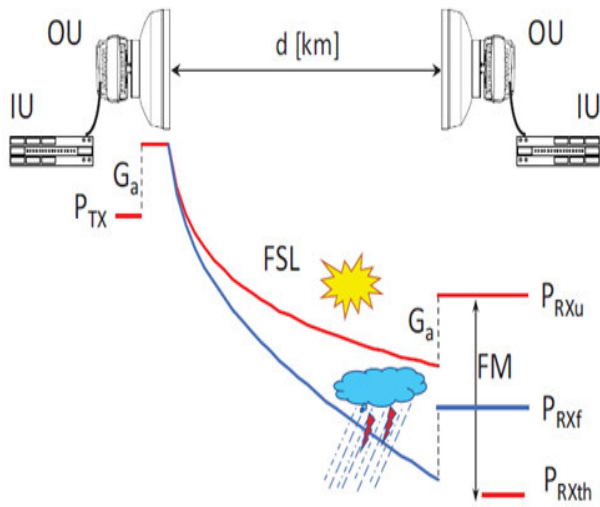


FIGURE 1. Link budget and fade margin calculation source [49].

D. ATMOSPHERIC GAS ATTENUATION

The attenuation caused by atmospheric gas is simplified and calculated by a model in accordance with the ITU-R P.676-10 recommendation [50]. As a result, the total attenuation A [dB] of the radio signal due to atmospheric gas can be calculated as follows:

$$Aa = \gamma d = (\gamma_o + \gamma_w) d \text{ [dB]} \tag{8}$$

where  $\gamma_o$  and  $\gamma_w$  are the specific attenuation for oxygen and water vapour, respectively, while  $d$  is the path length, for 38 GHz frequency, the attenuation due to atmospheric pressure is minimal due to the short distances between the receiver and access point.

E. RMS DELAY SPREAD

Extensive literature studies have revealed that in the time domain, the RMS delay spread increases more than the time duration of the sample ( $\delta\tau \gg T$ ), which influences the system’s key performance parameters. The cyclic prefix (CPs)

in the OFDM waveform is generally specified by the RMS delay spread or by the maximum excess delay of the wireless channel. It can mitigate inter-symbol interference (ISI) by concatenating cyclic prefixes (CPs) to data symbols at the expense of lower spectral efficiency [38]. The RMS is defined as:

$$\tau_{RMS} = \sqrt{\frac{\int_0^\infty (\tau - \tau')^2 p(\tau) d\tau}{\int_0^\infty p(\tau) d\tau}} \tag{9}$$

$$\tau' = \frac{\int_0^\infty \tau p(\tau) d\tau}{\int_0^\infty p(\tau) d\tau} \tag{10}$$

where  $p(\tau)$  is the power delay profile of the channel and  $\tau'$  is the average delay of the medium.

F. RICIAN K-FACTOR

Other than the path loss and shadowing effect, the transmitted wireless communication signals also suffer from different types of fading. The two distinct fading models are Rayleigh fading and Rician fading distribution with Rician factor K. The latter model is more widely used. Rician fading is caused by signal scattering. In the LOS case, the envelope of small-scale fading is predicted to track the Rician distribution. However, it occurs when one of the paths (characteristically, a LOS signal) is much stronger. The Rician K-factor characterises fast fading and represents the ratio of the strongest ray of multipath components (MPCs) power ( $P_{max}$ ) to the sum of other weaker (MPCs) power values, as follows

$$K = \frac{P_{max}}{P_{tot} - P_{max}} \tag{11}$$

where  $P_{tot}$  is the overall received power values from all multipath mechanisms. It has been noticed that the higher the K-factor, the lower the contribution of (MPCs) in the radio channel [23]. The proportion of power density scattered and absorbed by raindrops depends on the electrical dimension of the drops. Previously, multipath components were located in unobstructed LOS conditions during rain but not during dry periods. The K-factors have been employed to estimate whether the strong multipath components that cause fast fading occur in LOS and NLOS scenarios for outdoor. The results revealed that there is a strong association between the rain intensities (mm/h) and Rician factor (dB) [23], [24], as shown in (12):

$$K = 16.88 - 0.04R \text{ dB} \tag{12}$$

The Rician K-factor is inversely proportional to the rain rate. The results of [24] indicate that the coherent power decreases while the incoherently scattered power increases since the multipath power rises due to the increase in rain rate [24]. The mean and standard deviation of the received signal strength obtained from the measured data can also be utilised to predict the Rician factor, as shown by (13):

$$K = 10 \log_{10} \frac{\sqrt{\mu^2 - 6^2}}{\mu - \sqrt{\mu^2 - 6^2}} \text{ dB} \tag{13}$$

where  $\mu$  and  $\sigma^2$  are the mean and standard deviation of the received power calculated from the measured data, respectively. Notice that the higher the K-factor, the lower the contribution of MPCs in the radio channel. Since the measured LOS condition follows the short-addressed distance, the highest KF can be attributed to the dominant LOS component. This leads to a small DS which then justifies the solid and negative cross-correlation between DS and KF.

**IV. MEASUREMENTS OF RAIN RATE AND RAIN ATTENUATION**

This section highlights the use of an outdoor test link in Malaysia. The measurement experiments were performed in Universiti Teknologi Malaysia at Skudai Campus to investigate and analyses rain fade’s effect on mm-wave links for short-distance communications associated with rainfall intensities in tropical regions. A short path link operating at 38GHz horizontal polarisation was monitored for one year. The rainfall rate and received signal level have been measured simultaneously in 1-min time intervals for one year over a 300 m path length. The transmitter Tx and Rx hardware were placed between the Wireless Communication Research Lab (WCRL) and the Celcom Tower.

Figure 2 illustrates the top view of the location of the path link from Google Earth. The Tx latitudes and longitudes are (001 29 59 N and 103 43 10 E). The receiver was labelled Celcom Tower (001 28 24 N and 103 40 27 E).

The measurements were conducted in typical LOS at approximately 18m, and any barriers did not block the experimental radio path. The installation of the empirical link at 38 GHz, rain attenuation data logging system with the link has been illustrated in Figure 3.



**FIGURE 2. The top view of the location of the path link from Google Earth between the transmitter and receiver.**

Two types of data were collected. These are one-minute integration time rainfall rate (mm/h) and received signal level (RSL, dBm) data have been measured simultaneously, and satisfactory data availability of 98.6% was achieved. The physical parameters for the link are described in Table 2. The automatic gain control (AGC) output of the RF unit is interfaced with a personal computer which is equipped with a data acquisition card (PCL 818). The sampling interval of AGC level and it’s storing are controlled by a C-Language program

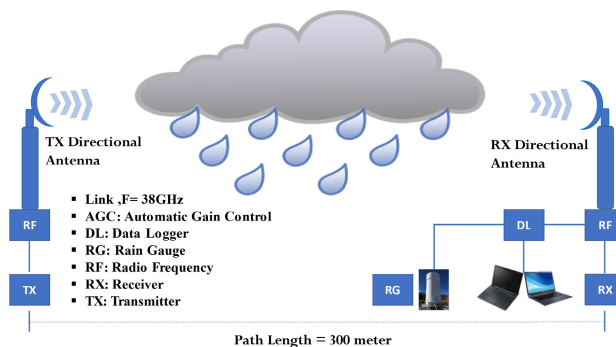


**FIGURE 3. The block diagram of the measurement equipment for data collection of rain rate and rain attenuation.**

running at PC. The AGC level is sampled every second. For raining event, the AGC level was set at some threshold level and the data were recorded every second below this level. For non-raining event, the AGC level is averaged and recorded every minute. Both PC and the Casella tipping bucket rain gauge RG were synchronised in time. Therefore, all raining events from RG data can be utilised to extract the AGC level variations corresponding to receive signal level variations of Radio Frequency RF signals during rains. The measurements were taken for 139 rainy events of this particular year for 6,341 rainy minutes and 46 minutes for each rainy event, including Malaysia’s Monsoon seasons. The program encountered a lower attenuation level value due to drizzling, which has not been recorded instantly by the rain gauge. The Received Signal Levels (RSL) dynamic range was 36.3 dB (varies from  $-25.3$  dBm to  $-61.6$  dBm) for the 38 GHz link. The front feed parabolic antennas were shaded by a wooden box and covered by radomes to exclude additional wet antenna attenuation during measurement.

**A. EXTRACTION OF RAIN RATE DATA**

The RG set upon the radio science lab roof. The Casella rain gauge is of the tipping bucket type, which is fitted with a solid-state logger. It is of three kinds. They are 0.1 mm, 0.2 mm and 0.5 mm sensitivity. A 0.5 mm sensitivity rain gauge gives better accuracy than the 0.1- and 0.2-mm rain gauges for medium and higher rainfall rates. Rainfall intensity from 150 mm/h to 200 mm/h, the errors encountered by 0.5 mm rain gauge is about 3%, while 0.2 mm and 0.1 mm rain gauges produce about 5% and 15% errors respectively during measurement. Therefore, the selection of a 0.5 mm sensitivity rain gauge is logical for the Malaysian tropical climate. The rain gauge’s availability is 100% because Casella is a compact unit equipped with inside batteries and consequently worked with 100%-time availability for most of the years. A MATLAB program has been used based on an algorithm developed to convert the recorded tipping time into one minute integration time, rain rate data for statistical analysis. The tipping time is not registered, and only the number of tips is counted and stored. This implies that the

one-minute rain rate will be read as a multiple of 30mm/hr. The cumulative distribution of one-year data is plotted in Figure 4 based on the one-minute average rain rate and the number of tips per minute. Referring to the latest ITU-R PN.837-17 prediction value, the proposed rain rate,  $R_{0.01}$  for Malaysia, is in the region of 90 mm/h. However, the measurement shows a higher value at 125mm/h

1) RAIN ATTENUATION MEASUREMENTS

The AGC level is sampled the received signal strength once per second. Thus, the MATLAB software processed the rain attenuation data via averaging the raw rain attenuation data for a continuous 60 second time length and recorded every minute to correlate between rain rate distribution along the propagation path and the attenuation of the received signal strength. These data have been processed to plot a continuous rain curve, which might be considered accurate above the 30 mm/hour rainfall rate. As a result, the maximum rain fades along 300 m terrestrial link at 38GHz for horizontally polarised can be computed as follows:

$$RSL_{during\ clear\ sky} - RSL_{during\ rainy\ conditions} [dB] \quad (14)$$

Figure 5 presents the complementary cumulative distribution function (CCDF) of the measured rain attenuation at 38 GHz over a 300 m path length at different time percentages (0.001% ≤ P ≤ 10%) for one year.

B. ATTENUATION VERSUS RAIN RATE

The rain rate and corresponding rain attenuation can be statistically extracted from equal probability values since both measurements are simultaneously conducted. Figure 6 presents the rain gauge measurements of the one-minute rain rate versus the rain attenuation at 38 GHz over 300 m. The degree of attenuation is strongly correlated to rain rate variations. The data indicates that in a 30 mm/h rain rate, the signal loss is about 4 dB over the 300 m path length. As the rain rate increases at 150 mm/h, the signal loss increases to more than 18 dB. Therefore, the average rain rate value of 125 mm/h was obtained at 0.01% of the time, and the corresponding rain attenuation is more than 15 dB at 38 GHz.

It should be noted that this attenuation was only found for the 300 m path length. However, it can be extrapolated as 50 dB/km over the 1 km actual path length since all researchers assumed rain intensity was uniform with a path length of less than 1 km. But This assumption does not hold for convective events, as the spatial decorrelation of the rain rate becomes steeper and steeper as the rain rate increases. As shown in Figure 5 the 300 m path length design at 38 GHz causes 29 dB loss for 0.001% outage.

V. RAIN ATTENUATION PREDICTION METHOD FOR MM-WAVE OVER A SHORT PATH LENGTH

The deviation between the practical measurement and the theoretical estimation of rain-induced attenuation at short-range links operating at lower mm-wave frequency bands (26 GHz and 38 GHz) have been analysed in [51] after

TABLE 2. Summary of main link parameter descriptions.

Link physical parameters	Specification
Frequency Band	37.0 - 39.5 GHz
Polarization	HP
Antenna type	Directional front feed parabolic antennas
Antenna Gain	44.9 dBi
Antenna beam width	2.3°
Maximum Tx Power dBm	15
Link length	300m
System bandwidth	28 MHz
Tx height	18.6m
Rx Antennas height	17.3m
Sensitivity	-61.6 dBm

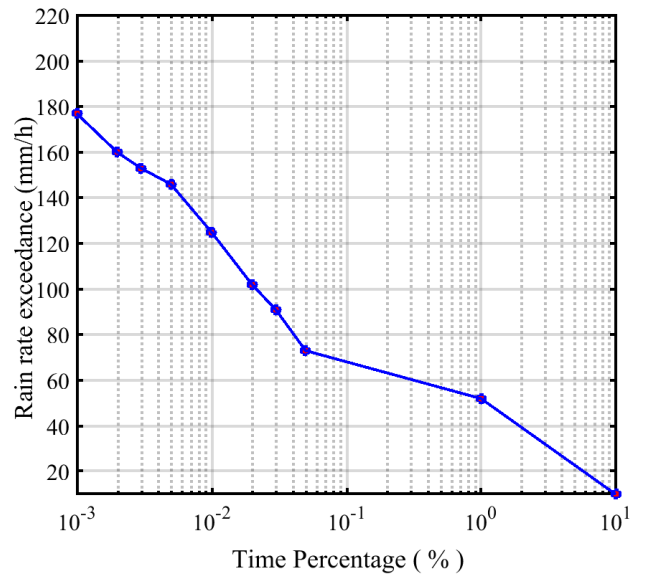


FIGURE 4. Cumulative distribution of the one-year measured rain rate.

excluding the wet antenna effects. In addition, the authors presented a modification for the attenuation prediction specified by the ITU-R P.530-17 model [52], as illustrated in the following formula:

$$A_{0.01} = k R_{0.01\%}^\alpha \times I_{f\gamma} \times d \quad (15)$$

where  $A_{0.01}$  is the estimated rain attenuation exceeding 0.01% of the time,  $d$  represents the actual path length and  $R_{0.01\%}$  is the measured rain intensity exceeding 0.01% of time.  $I_{f\gamma}$  is the proposed increment factor of specific attenuation at short communication path, as shown in (16) and (17). Factors  $k$  and  $\alpha$  are coefficients dependent on the raindrop size distribution of that particular location, the polarisation, rain temperature

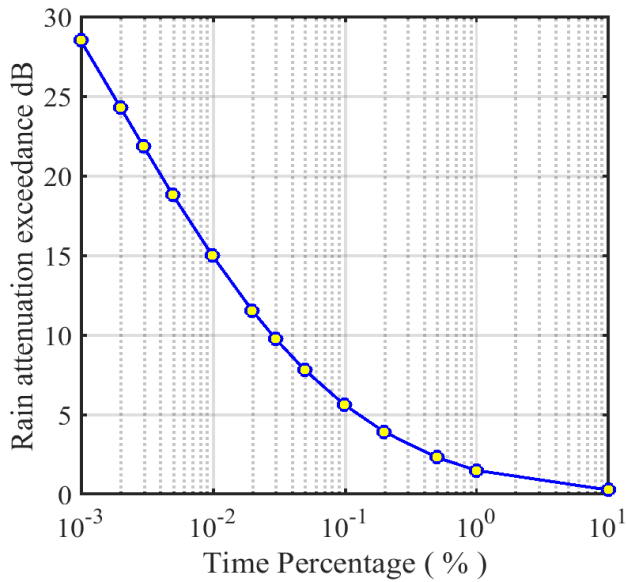


FIGURE 5. Cumulative distribution for the maximum rain attenuation at 300 m link.

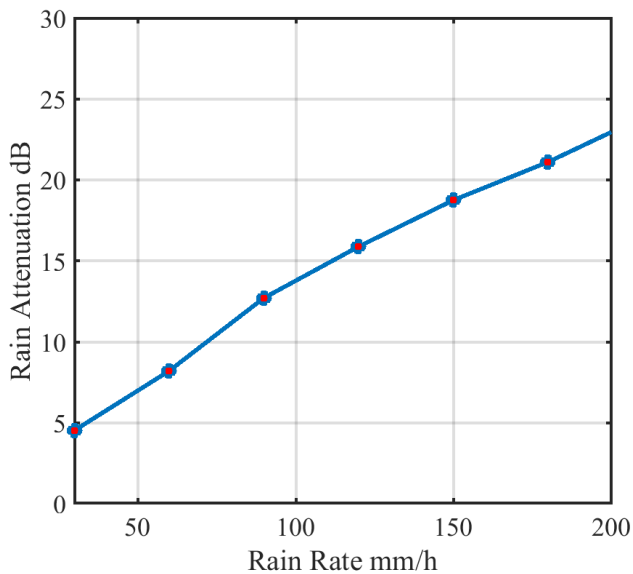


FIGURE 6. Cumulative distribution of measured rain rate of one year versus rain attenuation at 38 GHz over 300 m.

and frequency acquired from ITU P.838-3.

$$I_{f\gamma} = \left[ \frac{1}{1.77d^{0.77}R_{0.01}^{-0.05}} \right] \quad f \leq 40 \text{ GHz and } d < 1\text{km} \tag{16}$$

$$I_{f\gamma} = \left[ \frac{1}{0.477d^{0.633}R_{0.01}^{0.073}f^{0.123}} \right]^2 \quad \text{for } f > 40\text{GHz and } d < 1\text{km} \tag{17}$$

Table 3 and Figure 7 present a comparison between the predicted rain attenuation at frequencies <40 GHz based on Eq. 16 and experimental links. These are then measured at

different climate characteristics at 0.01% of the time. The rain fade predicted by applying the modified distance factor proposed in [51] provides higher consistency with the measured fade. In addition, the model’s performance was better when the path length was <700 m.

Similar measurements have been reported in South Korea for 75-GHz frequency over 100 m path length [28]. Measurements at 73/83 GHz of an installed 500 m terrestrial link were also accomplished by [53]. In Japan [31], rain attenuation data measured at 60 GHz over 150 m were compared with the predicted data proposed by the model in [51]. The results are displayed in Figure 8. The attenuation obtained by the proposed model in [51] matched the measured attenuation. The model’s performance presented in [51] is better at a shorter path length <700 m.

Figure 9 presents the rain attenuation versus the separation distance. The rain attenuation has been predicted using (15), (16) and (17) at the cell radius of 100-500 meters. As illustrated in Figure 9, the rain attenuation may exceed 14 dB over 200 m at 38 GHz using the proposed model. This will benefit the path loss analysis. Furthermore, the rain fades further increases by more than 5.35 dB when the cell size was changed from 100 m to 500 m for directional transmission. Thus, the proposed model seems to be an efficient tool for describing the coverage distance, spectral efficiency, throughput, capacity and outage probability for 5G LOS terrestrial outdoor short links located in Malaysia and different regions worldwide.

Figure 10 displays the distribution of several fading events for a given fade amplitude. The number of occurrences for rain attenuation is generated using received signal strength data measured for 12 months. The results indicate that at 38 GHz and 300 m path length, the number of fading events intensely decreases with fade amplitude. Figure 11 displays the probability of occurrences, which is considered a vital factor in the dynamic analysis of rain fade. The statistical distribution of rain fade over a short path at mm-wave frequencies depends on attenuation levels, location and climatic parameters. The statistical data contributes to system outages and availabilities caused by the link propagation and fade margins.

**A. LINK AVAILABILITY AND FADE MARGIN CALCULATION**

Link availability (A = 99.99%) for the annual time-frame includes outages due to rain and equipment failure [49]. The one-minute integration time for rain intensity (R > 125 mm/h) typical in tropical regions has also been considered. The atmospheric absorption at 38GHz was 0.08 dB/km (considered negligible). The link operates when the received signal power strength’s fade margin (FM) exceeds the rain and atmospheric attenuation. The fade margin values and the link-budget-calculator used during the planning phase have proven to deliver reliable availability and capacity [49], as follows:

$$FM [dB] > A_{0.01\%} + Aa \tag{18}$$

Here,  $A_{0.01\%}$  and  $A_a$  signify rain and atmospheric attenuation, respectively. Therefore, the atmospheric attenuation of 0.13 (dB/km) has a negligible impact on 38 GHz since it is relatively small. On the other hand, the average measured rain attenuation at 38 GHz is around 15 dB. Hence characterizing the channel statistically to derive valuable statistical properties distribution of the amplitude component is important when we look at the characterizing the performance of the wireless channel in rain scenario. Therefore, the probability that the rain-induced attenuation of the channel is worse than 15 (at  $R_{0.01} = 125$  mm/h) can be predicted as follows:

$$FA(a) = 2ae^{-a^2} \quad 0 \leq a \leq \infty \quad (19)$$

where  $a^2$  represents the channel's gain, hence attenuation more than 15 dB if the channel's amplitude is less than 0.1778. Hence, the probability that the attenuation of the wireless channel is worse than 15 dB is 0.0311. This indicates that the availability estimated with the measured rain rates was 99.968% for 300 m link in clear LOS with horizontally-polarised TX and RX antennas. It was found that the average link availability calculated with the measured rain rates is lower than those estimated in the link budgets [57].

The expected attenuation (tropical rain zone) has been computed for horizontal polarisation:

- ~ 26 dB @ 99.999% for 200 m link
- ~ 29.3 dB @ 99.999% for 300 m link

Hence, the link distance concerning the fade margin can be adjusted to optimise the availability of the point-to-point LOS millimetre wave link. After inserting the rain and atmospheric attenuation into (19), the maximum communication path length  $d$  can be numerically designed for a given  $R_{0.01\%}$  rain intensity when the transmit and receive antennas are horizontally polarised at 38 GHz. To achieve 99.99% availability and vertical polarisation, it is recommended that the 38 GHz links be confined to 177 m. The measurements indicate that the 38 GHz band can be used to fulfill high-capacity short-hop requirements. An extra 36.6 dB fade margin of rain attenuation should be considered to reach the same link quality for 300 m path length.

However, the reliability requirements of the mm-wave link do not only depend on the link margins. Therefore, the 99.999% reliability is more about the mean time between failures.

## VI. POWER DELAY PROFILE WITH CONSIDERATION OF THE WEATHER CONDITIONS OF KUALA LUMPUR CITY

The channel model has been created for simulation and analysis purposes. The power delay profile has been generated using the MATLAB code employed in the Version 2.0 NYUSIM software package. The key channel parameters have been estimated for cell sizes between 100-500 meters in UMi/LOS outdoor scenarios for omnidirectional and directional antenna types. By conducting extensive simulations under the weather conditions of Kuala Lumpur, the comprehensive effects of the directional and omnidirectional antenna on mm-wave channels have been investigated. The channel

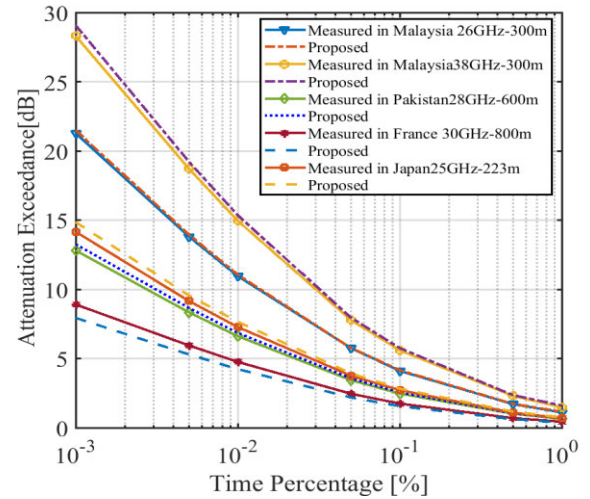


FIGURE 7. Measured and predicted rain attenuation using the proposed model in [51] at  $F < 40$  GHz and path length  $< 1$  km.

TABLE 3. Comparison of different rain attenuation studies at frequencies  $< 40$  GHz.

Region	Link parameters	Proposed $A_{0.01}$ dB	Measured $A_{0.01}$ dB
Malaysia	$f=38\text{GHz}$ , $d=300\text{m}$ , $R=125\text{mm/h}$ , Hp	15.4	15
Malaysia	$f=26\text{GHz}$ , $d=300\text{m}$ , $R=125\text{mm/h}$ Hp	11.1	10.5
Japan [54]	$f=25\text{GHz}$ $d=223$ m, $R=100\text{mm/h}$ , Hp	6.53	6.7
USA [24]	$f=38\text{GHz}$ $d=265$ m, $R=49\text{mm/h}$ , Vp	5.42	5.73
Pakistan [55]	$f=28\text{GHz}$ , $d=0.6\text{km}$ , $R_{0.01}=62\text{mm/h}$ , Hp	6.86	6.66
France [56]	$f=30\text{GHz}$ , $d=0.8\text{km}$ , $R_{0.01}=40\text{mm/h}$ , Vp	4.28	4.8

parameters such as received power, path loss, path loss exponent, RMS, delay spread, and Rician K-factor (KF) were analysed, to predict the best suitable cell size for tropical environments. Table 4 presents an extensive configuration of simulations and input parameters. The analysis results have been classified with the consideration of different factors, as follows:

### A. ANTENNA SETUP

The effect of antenna type on the mm-wave propagation channel has been explored for both omnidirectional and directional antenna transmissions of 24.6 dBi power gain and  $10^\circ$  beamwidths, with a transmit power of 15 dBm. There has been a general increase in RT and RX antenna gain by reducing the azimuth (the spread in the horizontal plane) and elevation (the spread in the z-direction) HPBW in NYUSIM (inverse relationship between HPBW and Tx, Rx antenna Gain).

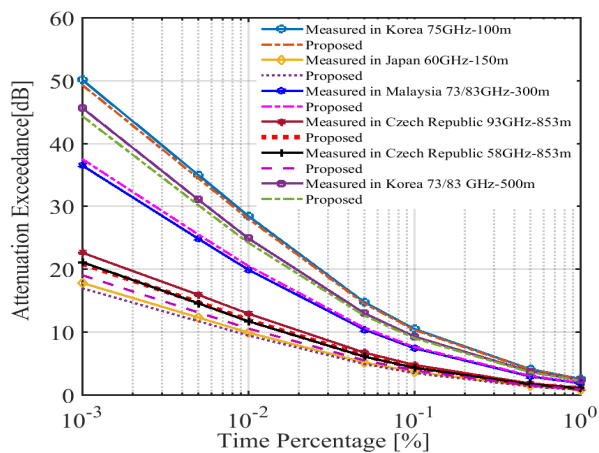


FIGURE 8. Measured and predicted rain attenuation using the proposed model in [51] at  $F > 40$  GHz and path length  $< 1$ km.

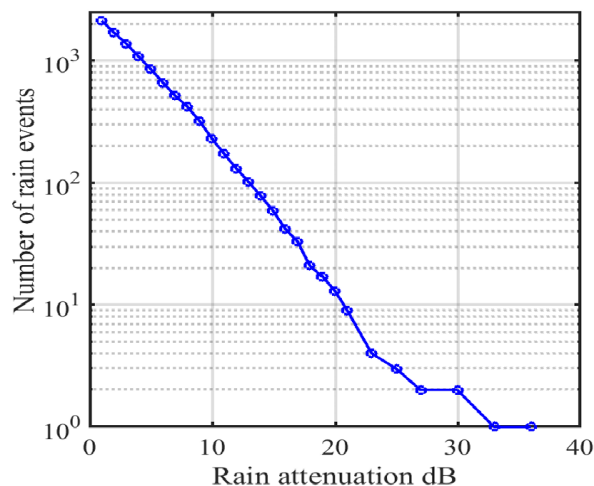


FIGURE 10. Total number of fading events for a given fade amplitude.

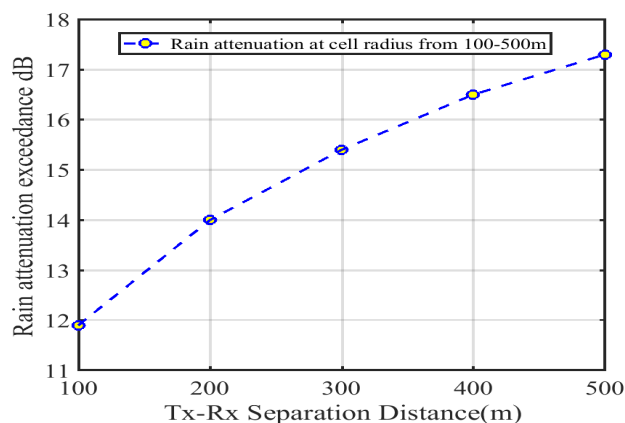


FIGURE 9. Predicted rain attenuation versus path length at cell radius from 100-500 meters using [62].

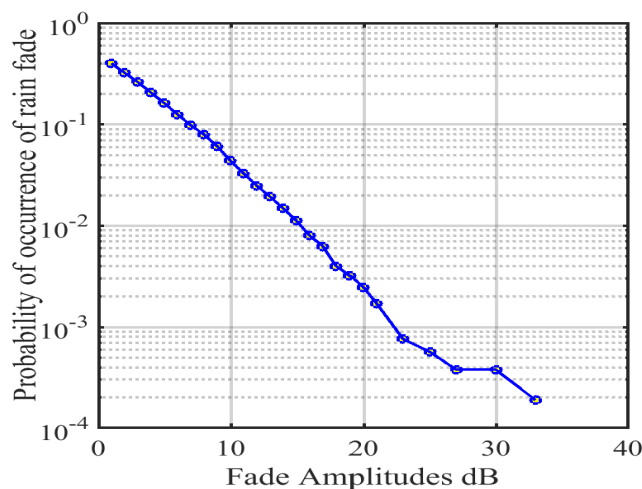


FIGURE 11. Probability of rain attenuation occurrences for different measured attenuation levels at 38 GHz and 300 m path length.

A comparison between the representative PDP for both omnidirectional and directional antenna transmissions with and without rain fade for urban microcells at 38 GHz is presented in Figures 12-15. The figures illustrate the required system parameters for better performance in tropical climates. From the obtained PDP, we can estimate the power intensity and time delay of each signal copy. We can also extract some information during rainfall. The graphs show the variation of the received power and how the received power varies with time. It is clear that at the same frequency band (38 GHz), the representative PDP is dramatically affected by rainfall according to the measurement of  $R_{0.01\%}$  (mm/h) in Malaysia. A 6.3 dB drop in the omnidirectional received power has been observed during the receiver’s transition from clear sky to rain scenarios. In comparison, the simulation results revealed a difference between the received signal (with and without rain attenuation) of about 17.9 dB in the directional antenna. The percentage of path loss in the directional antenna is higher by approximately 35% than the omnidirectional antenna.

In Figures 13, the value of large-scale path loss for directional and PDP considering rain attenuation equals 137.1 dB. Thus, the signal will be exposed to the attenuation by almost more than 17.9 dB when it propagates during rain in the LOS scenario. In contrast, for the omnidirectional PDP, the value of path loss is equal to 119.3dB and the signal will be attenuated by only 6.3 dB when it propagates during rain in the LOS scenario. Additionally, the obtained PLE for the directional and omnidirectional profile at 38 GHz is equal to 2.9 and 2.2, respectively.

It can be observed that the multipath components rise during rain, as shown in Figure 12 compared to Figure 13. This multipath may be due to diffraction, reflection, or scattering of large raindrops in tropical regions. The rainfall induces an additional loss on the multipath components compared to no rainfall, as shown in Figure 13. The figures also show a 3.5–9 ns reduction in the RMS delay spread for rain propagation conditions. This is due to the relative decrease in the

**TABLE 4.** Detailed configuration of NYUSIM simulations.

Input Channel Parameters	Value(s)
The carrier frequency in GHz (0.5-100 GHz)	38 GHz
RF bandwidth in MHz (0-1000 MHz)	800 MHz
The operating scenario can be UMi, UMa or RMa	UMi
The operating environment can be LOS or NLOS	LOS
Minimum and maximum separation distance Tx-Rx	100-500 m
Transmit power in dBm	15 dBm
Tx transmits antenna height	17.3m
Rx receiver antenna height	1.5m
Barometric Pressure in mbar ( $1e^{-5}$ to 1013.25 mbar)	1010.00
Humidity in % (0-100%)	85%
The temperature in degree Celsius	28 <sup>c</sup>
Rain rate in mm/hr (0-150 mm/hr)	125mm/hr
Polarisation (Co-Pol or X-Pol)	Co-Pol
Transmit-receive array type (ULA or URA)	ULA
Number of transmit antenna elements (1-128)	1
Number of receive antenna elements (1-64)	1
Tx, Rx antenna Gain	24dBi
Receive antenna azimuth HPBW in degrees (7-360°)	TX = 10 RX = 10
Receive antenna elevation HPBW in degrees (7-45°)	
Antenna types	Directional Omnidirectional

strength of the multipath components compared to the dominant component in PDP due to the influence of rainfall [72].

The directional antennas effectively reduce the delay spread and direct the antenna beams to the right angle. In contrast, omnidirectional transmission introduces a long delay spread compared to the directional antenna, with and without considering rain attenuation, as illustrated in Figures 14 and 15. The difference is an average of around 15 ns. This is mainly due to multipath components arriving from several dissimilar scattering and reflection mechanisms for LOS and NLOS scenarios. Hence, the number of stronger received signals produced by a few solid multipath components arriving at the receiver will decrease.

Figures 12 and 13 show that the directional antenna boosts the received power, path loss and path loss exponent but dramatically reduces the RMS delay. This indicates that directional mm-wave systems can help avoid ISI to achieve higher system performance. The directional channel induces more losses when compared to the omnidirectional channel. However, the received power increases since most reflections and scattering will fall outside the antenna's beamwidth when the directional antenna is used. In addition, the wide beam antenna provides less path loss compared to the narrow beam antenna.

### B. TX-RX SEPARATION DISTANCES

When the TX-RX separation distance increases beyond 300 meters, the number of receivable multipath components

decreases due to the attenuation of travelling through long paths. The received signal from the multipath drops below system sensitivity.

Based on The CI model utilized by the NYUSIM simulations, the critical parameter of the propagation channel at 38 GHz, such as PL and PLE, dramatically increases with increasing TX to RX separation distance, as illustrated PL profile in Figures 16 and 17. The simulation results were obtained by comparing the directional and omnidirectional PL models considering meteorological factors of Kuala Lumpur. The PL is estimated at a TX height of 17.3 m and an RX height of 1.5 m with co-polarised antenna configurations. The omnidirectional model was obtained by removing the effects of TX and RX antenna gains.

Figures 16 and 17 present an immediate equal of free space path loss during the clear sky condition for the directional and omnidirectional path losses of LOS optioned from CI model. The PLE in the LOS environment at 38 GHz was found to be  $n = 2$ , relatively close to the expected theoretical free space for PLE ( $n$ ) of 2 during the clear sky condition. However, the PLE ( $n$ ) of 2.78 was obtained using (4) and the measured data by considering the rain condition. The PLE is noted to have a monotonically decreasing rate of received signal strength where the value of PLE relies on the propagation area.

The large-scale PL model in the NYUSIM simulation result was around 126.23 dB by considering the rain attenuation effects on the 300m at 38 GHz LOS terrestrial link.

The RMS delay spread and received power level further decrease with the increase of TX–RX separation ( $d$ ). The difference in RMS delay was more than 3.5 ns when the cell size changed from 100 m to 500 m for directional transmission. The TX–RX separation distance increment causes the path loss to increase and become higher than the dynamic range. This will consequently lead to fewer detectable multipath components, causing more negligible RMS delay spreads. The findings are consistent with reported outcomes in the literature [22], [58]. The RMS delay spread is inversely proportional to the TX-RX separation distance [32].

### C. RAIN ATTENUATION

During rain, the mm-wave directional and omnidirectional channels predominantly suffer from raindrop scattering rather than absorption. The rain fade causes additional diffused scattering during the propagation of mm-wave signals. This consequently creates a weaker path that is undetectable by the receiver. The received power level decreases as the rain rate gradually increases. A series of deep fading predicted at the cell radius of 200 m is around 10 dB at the rain intensity of 125 mm/h. The comprehensive analysis of rain fade characteristics indicates that the received signal envelope fades out much more during the day than at night because of the high probability of rain. It has been observed that severe path loss is more likely to occur between 14:00 and 15:00. Less path loss was noticed during the hours of [00:00, 08:00] and [20:00-24:00] since rain events are relatively rare in those times compared to the intervals of [12:00, 16:00]

Directional PDP with Strongest Power (Kuala Lumpur at with a clear sky)

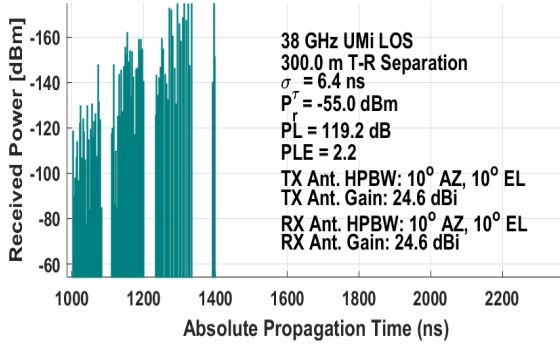


FIGURE 12. Directional PDP at clear sky status.

Omnidirectional Power Delay Profile PDP(Kuala Lumpur at a clear sky)

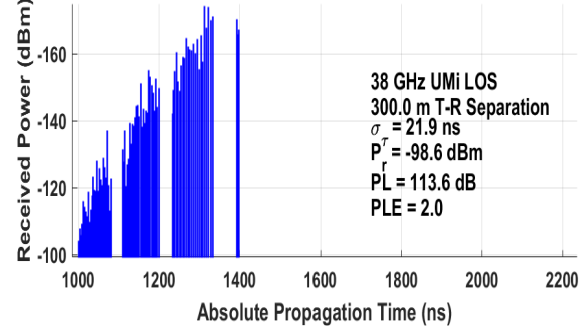


FIGURE 14. Omnidirectional PDP at clear sky status.

Directional PDP with Strongest Power (Kuala Lumpur at R=125 mm/h)

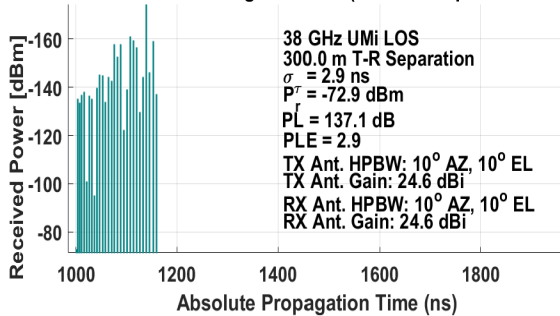


FIGURE 13. Directional PDP at heavy rain status.

Omnidirectional Power Delay Profile (PDP)

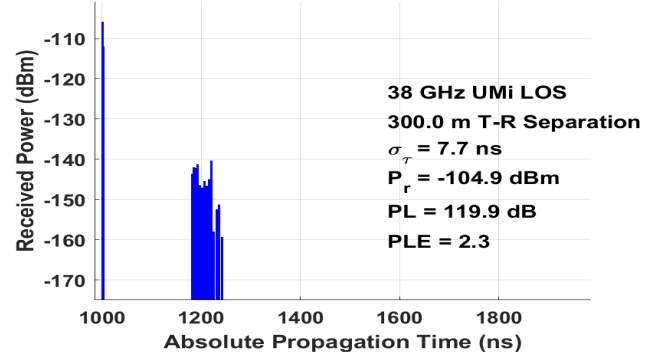


FIGURE 15. Omnidirectional PDP at heavy rain status.

and [16:00, 20:00]. The number of significant multipath components increases during rain, decreasing the received power [34], [76]. The RMS delay and angular spread also reduce.

It has been validated that the power of the LOS component decreases as the multipath power increases at some point during the rain events. This is because when rain intensity increases, the rain attenuation correspondingly rises. As a result, the coherent power will decrease, and the incoherently scattered power will increase. The mean and standard deviation of the RSS from the measured data may estimate the Rician K factor suitable for the wireless link when considering the different meteorological factors. The results indicate that the Rician K-factor decreases when rain attenuation is considered. This outcome is similar to the results presented in [29]. Rain attenuation is more critical than the separation distance when determining the RMS delay spread in tropical climates. The performance of the mm-wave link is significantly affected by rain fade more than the increased distance between TX and RX. The channel model employed in this paper underestimates the RF attenuation of tropical regions compared to actual measured data by almost more than 6dB. This is justified because the current NYUSIM software package Version 2.0 considered the Laws & Parsons' rainfall DSD model to predict rain fade over mm-wave frequencies.

However, this model is deemed more appropriate for temperate regions and unsuitable for areas outside of Europe and North America to examine the relationship between raindrop size and rain intensity. Hence, we propose replacing the Laws and Parsons' rainfall model with Mie scattering approaches to predict attenuation at higher frequencies used by new systems with a larger bandwidth. This will be more accurate for defining link distances and the needed SNR to compensate for the unsatisfactory fading events in tropical regions.

#### D. IMPACT OF ANTENNA HEIGHT

The RMS delay spread has been compared for three antenna heights. It was found that the delay spread significantly increases with antenna height. The PLE tends to have lower values at higher antenna heights since the blockage effect is reduced, and better ground clearance can be obtained to produce a similar performance to LOS.

#### E. IMPACT OF ANTENNA GAIN

The received signal level was significantly affected by the antenna gain. On the other hand, the PL is unrelated to the antenna gain. It was noticed that the receiver's antenna gain is inversely proportional to the RMS delay. A lower gain of 15-dBi at the RX antenna has a higher RMS delay spread at smaller TX-RX separation than the 24-dBi antenna.

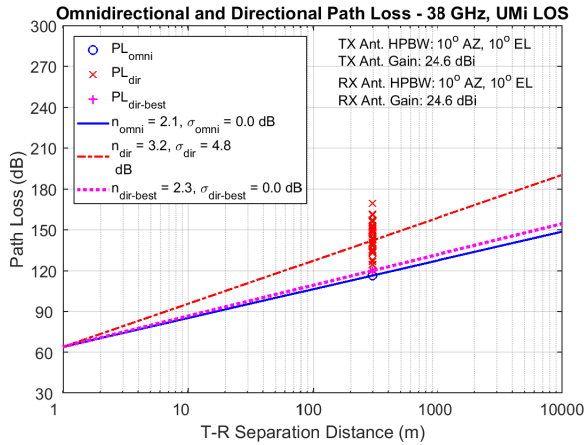


FIGURE 16. CI path loss model at 38 GHz for outdoor D2D link with 28°C sunny sky (htx = 17.3, hrx = 1.5 m).

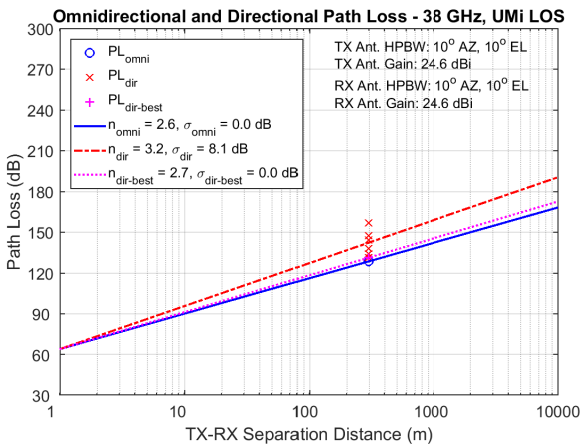


FIGURE 17. CI path loss model at 38 GHz for outdoor D2D link with a rain rate of 125 mm/h (htx = 17.3, hrx = 1.5 m).

However, the lower gain of the RX antenna has a shorter RMS delay spread at areas with longer TX-RX separation distance [22], [57].

F. THE IMPACT OF FREQUENCY BANDS

The RMS delay spread and the received signal generally decrease with the increase in frequency. The PL also increases with frequency. As expected, the PLE at higher frequencies tends to be higher as well. The RMS delay at 28 GHz was found to increase compared to 38 GHz. However, when the delay spread is much lower, the symbol time is likewise much shorter due to the large bandwidth at the mm-wave [59]. The values of the Rician K-factor also increase with frequency [8].

VII. CONCLUSION

This work has analysed the measurements of the one-year rain rate and its effect on 38 GHz links over 300 m path length. The statistical distributions of the rain rate and rain attenuation have been presented. The average rain rate value of 125 mm/h was found at 0.01% of the time, and the

corresponding rain attenuation was more than 15 dB at 38 GHz. A method based on distance factor modifications has been discussed and evaluated according to the ITU-R P.530-17 for rain attenuation prediction at mm-wave over a short path length. The rain fade predicted by applying the modified distance factor is highly consistent with the measured fade. The performance of the model was better when the path length was <700 m. The probability of rain attenuation occurrences for different measured attenuation levels at 38 GHz and 300 m path length has been presented. Based on outdoor microcellular measurements in Malaysia, the average path loss and path loss exponent have been calculated. This study further considered the rain cell radius and rainfall intensity to determine the variance between the LOS path loss and received signal during clear skies and rain from the representative PDP. The NYUSIM channel model simulator has been employed to explore its effectiveness in characterising the impact of rain attenuation on large-scale parameters of mm-wave propagation channels in tropical climates. The NYUSIM channel model underestimated AT's attenuation factor in tropical regions, significantly influencing the most critical channel properties such as the RMS delay spread and LOS component Rician K-factor (KF).

Moreover, the NYUSIM channel model did not properly work for path loss prediction in tropical climates. The excess path loss and high delay-spread values have the most severe propagation impairments, especially when considering the deployment of 5G systems in tropical environments with heavy rainfall. Within 200 m transceiver distances, the effect of rain attenuation on line-of-sight path loss can be considered when the difference between clear skies and rain is greater than 1 dB. These comprehensive simulation results are valuable for designing future mobile broadband for outdoor applications. As previously noted, empirical investigations should encompass actual measurements of outdoor tropical climates and not just focus on data contents from simulation software. In future works, the close-in path loss model will be modified.

APPENDIX

Acronym	Full form
5G	Fifth Generation.
3GPP	3rd Generation Partner Project.
BER	Bit Error Rate.
CIR	Channel Impulse Response.
FSL	Free-Space Loss.
ITU-R	International Telecommunication.
Union	Recommendation.
MIMO	Multiple Inputs and Multiple Outputs.
OFDM	Orthogonal Frequency Division Multiplexing.
NLOS	Non-Line-of-Sight.
ULA	Uniform Liner Array.
URA	Uniform Rectangular Array.
HPBW	Half-Power Beamwidth.
UMi	Urban Microcell.
UMa	Urban Microcell.

RMa	Rural Macrocell.
Co-Pol	Co-Polarised.
X-Pol	Cross-Polarised.
PLE	Path Loss Exponent.
RMS	Root-Mean-Square.
ISI	Inter Sample Interference.
KF	Rician K-Factor.
FM	Fade Margin.
CPs	Cyclic Prefix.
MPC	Multipath Components.
AT	Attenuation Factor.
PDP	Power Delay Profile.
CW	Continuous Wave.
SF	Shadow Fading.
SSCM	Statistical Spatial Channel Model.
O2I	Outdoor-to-Indoor.
PER	Packet Error Rate.
SINR	Signal to Interference Plus Noise Ratio.
DS	Delay Spread.
SUI	Stanford University Interim.
ABG	Alpha-Beta-Gamma.
DSD	Drop size Distribution.

## ACKNOWLEDGMENT

The authors are grateful to the International Islamic University Malaysia (IIUM) and the College of Electrical & Electronics Technology of Benghazi, Libya, for supporting this research. The authors would also like to acknowledge the support provided by the Ministry of Higher Education Malaysia (MOHE) under the Fundamental Research Grant Scheme (FRGS/1/2019/TK04/UTM/02/34), and in part by Universiti Teknologi Malaysia (UTM) under the Collaborative Research Grant (CRG) of R.J130000.7351.4B468, and the Higher Institution Centre of Excellence (HICOE) Grants of R.J130000.7851.4J413 and R.J130000.7851.4J493. It was also supported in part by the Universiti Sains Islam Malaysia (USIM), Malaysia.

## REFERENCES

- [1] I. Shayea, T. A. Rahman, M. H. Azmi, and M. R. Islam, "Real measurement study for rain rate and rain attenuation conducted over 26 GHz microwave 5G link system in Malaysia," *IEEE Access*, vol. 6, pp. 19044–19064, 2018.
- [2] D. Wu, J. Wang, Y. Cai, and M. Guizani, "Millimeter-wave multimedia communications: Challenges, methodology, and applications," *IEEE Commun. Mag.*, vol. 53, no. 1, pp. 232–238, Jan. 2015.
- [3] I. Shayea, M. Ergen, M. H. Azmi, S. A. Çolak, R. Nordin, and Y. I. Daradkeh, "Key challenges, drivers and solutions for mobility management in 5G networks: A survey," *IEEE Access*, vol. 8, pp. 172534–172552, 2020.
- [4] A. A. Budalal, M. R. Islam, M. H. Habaebi, and T. A. Rahman, "Millimeter wave channel modeling—Present development and challenges in tropical areas," in *Proc. 7th Int. Conf. Comput. Commun. Eng. (IC3CE)*, Sep. 2018, pp. 23–28.
- [5] E. Gures, I. Shayea, A. Alhammedi, M. Ergen, and H. Mohamad, "A comprehensive survey on mobility management in 5G heterogeneous networks: Architectures, challenges and solutions," *IEEE Access*, vol. 8, pp. 195883–195913, 2020.
- [6] P. Zhang, B. Yang, C. Yi, H. Wang, and X. You, "Measurement-based 5G millimeter-wave propagation characterization in vegetated suburban macrocell environments," *IEEE Trans. Antennas Propag.*, vol. 68, no. 7, pp. 5556–5567, Jul. 2020.
- [7] A. N. Uwaechia and N. M. Mahyuddin, "A comprehensive survey on millimeter wave communications for fifth-generation wireless networks: Feasibility and challenges," *IEEE Access*, vol. 8, pp. 62367–62414, 2020.
- [8] Z. Lai, H. Yi, K. Guan, B. Ai, W. Zhong, J. Dou, Y. Zeng, and Z. Zhong, "Impact of meteorological attenuation on channel characterization at 300 GHz," *Electronics*, vol. 9, no. 7, p. 1115, Jul. 2020.
- [9] I. A. Hemadeh, K. Satyanarayana, M. El-Hajjar, and L. Hanzo, "Millimeter-wave communications: Physical channel models, design considerations, antenna constructions, and link-budget," *IEEE Commun. Surveys Tuts.*, vol. 20, no. 2, pp. 870–913, 2nd Quart., 2018.
- [10] A. B. Surahio, S. Hafeez, and N. Bohra, "Analyzing indoor/outdoor environmental effects with varying cell size on 5G millimeter-wave propagation," in *Proc. 3rd Int. Conf. Comput., Math. Technol. (iCoMET)*, Jan. 2020, pp. 1–8.
- [11] T. S. Rappaport, S. Sun, R. Mayzus, H. Zhao, Y. Azar, K. Wang, G. N. Wong, J. K. Schulz, M. Samimi, and F. Gutierrez, "Millimeter wave mobile communications for 5G cellular: It will work!" *IEEE Access*, vol. 1, pp. 335–349, 2013.
- [12] T. S. Rappaport, G. R. Maccartney, M. K. Samimi, and S. Sun, "Wideband millimeter-wave propagation measurements and channel models for future wireless communication system design," *IEEE Trans. Commun.*, vol. 63, no. 9, pp. 3029–3056, Sep. 2015.
- [13] P. Zhang, J. Li, H. Wang, and X. You, "Millimeter-wave space-time propagation characteristics in urban macrocell scenarios," in *Proc. IEEE Int. Conf. Commun. (ICC)*, May 2019, pp. 1–6.
- [14] J. Li, P. Zhang, H. Wang, C. Yu, and W. Hong, "High-efficiency millimeter-wave wideband channel measurement system," in *Proc. Eur. Conf. Antennas Propag. (EuCAP)*, 2019, pp. 1–5.
- [15] C. U. Bas, R. Wang, D. Psychoudakis, T. Henige, R. Monroe, J. Park, J. Zhang, and A. F. Molisch, "A real-time millimeter-wave phased array MIMO channel sounder," in *Proc. IEEE 86th Veh. Technol. Conf. (VTC-Fall)*, Sep. 2017, pp. 1–6.
- [16] S. Geng, J. Kivinen, X. Zhao, and P. Vainikainen, "Millimeter-wave propagation channel characterization for short-range wireless communications," *IEEE Trans. Veh. Technol.*, vol. 58, no. 1, pp. 3–13, Jan. 2009.
- [17] X. Zhao, S. Li, Q. Wang, M. Wang, S. Sun, and W. Hong, "Channel measurements, modeling, simulation and validation at 32 GHz in outdoor microcells for 5G radio systems," *IEEE Access*, vol. 5, pp. 1062–1072, 2017.
- [18] *Technical Specification Group Radio Access Network; Study on 3D Channel Model for LTE (Release 12)*, document TR 36.873 V12.2.0, 3GPP, France, 2015.
- [19] Á. Drozdy, P. Kántor, and J. Bitó, "Effects of rain fading in 5G millimeter wavelength mesh networks," in *Proc. 10th Eur. Conf. Antennas Propag. (EuCAP)*, Apr. 2016, pp. 1–5.
- [20] A. M. Al-Samman, T. A. Rahman, M. H. Azmi, and M. N. Hindia, "Large-scale path loss models and time dispersion in an outdoor line-of-sight environment for 5G wireless communications," *AEU-Int. J. Electron. Commun.*, vol. 70, no. 11, pp. 1515–1521, Nov. 2016.
- [21] A. M. Al-Samman, M. N. Hindia, and T. A. Rahman, "Path loss model in outdoor environment at 32 GHz for 5G system," in *Proc. IEEE 3rd Int. Symp. Telecommun. Technol. (ISTT)*, Nov. 2016, pp. 9–13.
- [22] T. S. Rappaport, F. Gutierrez, Jr., E. Ben-Dor, J. N. Murdock, Y. Qiao, and J. I. Tamir, "Broadband millimeter-wave propagation measurements and models using adaptive-beam antennas for outdoor urban cellular communications," *IEEE Trans. Antennas Propag.*, vol. 61, no. 4, pp. 1850–1859, Apr. 2013.
- [23] A. D. Panagopoulos, K. P. Liolis, and P. G. Cottis, "Rician K-factor distribution in broadband fixed wireless access channels under rain fades," *IEEE Commun. Lett.*, vol. 11, no. 4, pp. 301–303, Apr. 2007.
- [24] H. Xu, T. S. Rappaport, R. J. Boyle, and J. H. Schaffner, "Measurements and models for 38-GHz point-to-multipoint radiowave propagation," *IEEE J. Sel. Areas Commun.*, vol. 18, no. 3, pp. 310–321, Mar. 2000.
- [25] J. Huang, Y. Cao, X. Raimundo, A. Cheema, and S. Salous, "Rain statistics investigation and rain attenuation modeling for millimeter wave short-range fixed links," *IEEE Access*, vol. 7, pp. 156110–156120, 2019.
- [26] L. Luini, G. Roveda, M. Zaffaroni, M. Costa, and C. G. Riva, "The impact of rain on short E-band radio links for 5G mobile systems: Experimental results and prediction models," *IEEE Trans. Antennas Propag.*, vol. 68, no. 4, pp. 3124–3134, Apr. 2020.
- [27] Á. Faragó, P. Kántor, and J. Z. Bitó, "Rain effects on 5G millimeter wave ad-hoc mesh networks investigated with different rain models," *Periodica Polytechnica Electr. Eng. Comput. Sci.*, vol. 60, no. 1, pp. 44–50, 2016.

- [28] S. Shrestha and D. Y. Choi, "Rain attenuation statistics over millimeter wave bands in South Korea," *J. Atmos. Sol.-Terr. Phys.*, vols. 152–153, pp. 1–10, Jan. 2017.
- [29] E. Hong, S. Lane, D. Murrell, N. Tarasenko, and C. Christodoulou, "Terrestrial link rain attenuation measurements at 84 GHz," in *Proc. United States Nat. Committee, URSI Nat. Radio Sci. Meeting (USNC-URSI NRSIM)*, Jan. 2017, pp. 1–2.
- [30] P. Valtr and P. Pečač, "On distance factor in rain attenuation predictions," in *Proc. 13th Eur. Conf. Antennas Propag. (EuCAP)*, 2019, pp. 1–3.
- [31] J. H. Kim, M.-W. Jung, Y. K. Yoon, and Y. J. Chong, "The measurements of rain attenuation for terrestrial link at millimeter wave," in *Proc. Int. Conf. ICT Converg. (ICTC)*, Oct. 2013, pp. 848–849.
- [32] E. S. Hong, S. Lane, D. Murrell, N. Tarasenko, C. Christodoulou, and J. Keeley, "Estimating rain attenuation at 72 and 84 GHz from raindrop size distribution measurements in Albuquerque, NM, USA," *IEEE Geosci. Remote Sens. Lett.*, vol. 16, no. 8, pp. 1175–1179, Aug. 2019.
- [33] A. Hirata, R. Yamaguchi, H. Takahashi, T. Kosugi, K. Murata, N. Kukutsu, and Y. Kado, "Effect of rain attenuation for a 10-Gb/s 120-GHz-band millimeter-wave wireless link," *IEEE Trans. Microw. Theory Techn.*, vol. 57, no. 12, pp. 3099–3105, Dec. 2009.
- [34] V. Kvicera and M. Grabner, "Rain attenuation at 58 GHz: Prediction versus long-term trial results," *EURASIP J. Wireless Commun. Netw.*, vol. 2007, no. 1, pp. 1–7, Dec. 2007.
- [35] J. M. García-Rubia, J. M. Riera, P. Garcia-del-Pino, and A. Benarroch, "Attenuation measurements and propagation modeling in the W-band," *IEEE Trans. Antennas Propag.*, vol. 61, no. 4, pp. 1860–1867, Apr. 2013.
- [36] N. Daoud, C. Christodoulou, D. Murrell, N. Tarasenko, E. Hong, and S. Lane, "Rain attenuation analysis at 84 GHz," in *Proc. IEEE Int. Symp. Antennas Propag., USNC/URSI Nat. Radio Sci. Meeting*, Jul. 2017, pp. 1629–1630.
- [37] G. R. MacCartney and T. S. Rappaport, "Study on 3GPP rural macrocell path loss models for millimeter wave wireless communications," in *Proc. IEEE Int. Conf. Commun. (ICC)*, May 2017, pp. 1–7.
- [38] G. R. MacCartney, T. S. Rappaport, S. Sun, and S. Deng, "Indoor office wideband millimeter-wave propagation measurements and channel models at 28 and 73 GHz for ultra-dense 5G wireless networks," *IEEE Access*, vol. 3, pp. 2388–2424, 2015.
- [39] S. Lee, C. Cho, E.-K. Hong, and B. Yoon, "Forecasting mobile broadband traffic: Application of scenario analysis and Delphi method," *Expert Syst. Appl.*, vol. 44, pp. 126–137, Feb. 2016.
- [40] M. K. Samimi and T. S. Rappaport, "3-D millimeter-wave statistical channel model for 5G wireless system design," *IEEE Trans. Microw. Theory Techn.*, vol. 64, no. 7, pp. 2207–2225, Jul. 2016.
- [41] S. Sun, G. R. MacCartney, M. K. Samimi, and T. S. Rappaport, "Synthesizing omnidirectional antenna patterns, received power and path loss from directional antennas for 5G millimeter-wave communications," in *Proc. IEEE Global Commun. Conf. (GLOBECOM)*, Dec. 2015, pp. 1–7.
- [42] G. R. MacCartney, S. Sun, T. S. Rappaport, Y. Xing, H. Yan, J. Koka, R. Wang, and D. Yu, "Millimeter wave wireless communications: New results for rural connectivity," in *Proc. 5th Workshop All Things Cellular, Oper., Appl. Challenges*, Oct. 2016, pp. 31–36.
- [43] M. K. Samimi and T. S. Rappaport, "Local multipath model parameters for generating 5G millimeter-wave 3GPP-like channel impulse response," in *Proc. 10th Eur. Conf. Antennas Propag. (EuCAP)*, Apr. 2016, pp. 1–5.
- [44] S. Sun, G. R. MacCartney, and T. S. Rappaport, "A novel millimeter-wave channel simulator and applications for 5G wireless communications," in *Proc. IEEE Int. Conf. Commun. (ICC)*, May 2017, pp. 1–7.
- [45] S. Ju, O. Kanhere, Y. Xing, and T. S. Rappaport, "A millimeter-wave channel simulator NYUSIM with spatial consistency and human blockage," in *Proc. IEEE Global Commun. Conf. (GLOBECOM)*, Dec. 2019, pp. 1–6.
- [46] O. O. Erunkulu, A. M. Zungeru, C. K. Lebekwe, and J. M. Chuma, "Cellular communications coverage prediction techniques: A survey and comparison," *IEEE Access*, vol. 8, pp. 113052–113077, 2020.
- [47] A. Morgado, K. M. S. Huq, S. Mumtaz, and J. Rodriguez, "A survey of 5G technologies: Regulatory, standardization and industrial perspectives," *Digit. Commun. Netw.*, vol. 4, no. 2, pp. 87–97, Apr. 2018.
- [48] M. Shafi, J. Zhang, H. Tataria, A. F. Molisch, S. Sun, T. S. Rappaport, F. Tufvesson, S. Wu, and K. Kitao, "Microwave vs. millimeter-wave propagation channels: Key differences and impact on 5G cellular systems," *IEEE Commun. Mag.*, vol. 56, no. 12, pp. 14–20, Dec. 2018.
- [49] A. Hilt, "Availability and fade margin calculations for 5G microwave and millimeter-wave anyhaul links," *Appl. Sci.*, vol. 9, no. 23, p. 5240, Dec. 2019.
- [50] *IPrediction Procedure for the Evaluation of Interference Between Stations on the Surface of the Earth at Frequencies Above About 0.1 GHz*, document Rec. ITU-R P.452-16, TU-R, 2015.
- [51] A. A. H. Budalal, M. R. Islam, K. Abdullah, and T. A. Rahman, "Modification of distance factor in rain attenuation prediction for short-range millimeter-wave links," *IEEE Antennas Wireless Propag. Lett.*, vol. 19, no. 6, pp. 1027–1031, Jun. 2020.
- [52] *Propagation Data and Prediction Methods Required for the Design of Terrestrial Line-of-Sight Systems*, document Rec. ITU-R, P 530-12, 2012.
- [53] W. Chujo, T. Manabe, and S.-I. Yamamoto, "60-GHz short-range terrestrial rainfall attenuation compared with K-band long-distance satellite link," in *Proc. Int. Symp. Antennas Propag. Conf.*, Dec. 2014, pp. 559–560.
- [54] M. M. Hasan, R. Jayawardene, T. Hirano, J. Hirokawa, and M. Ando, "Localisation of rain and its effect on propagation in Tokyo tech millimeter-wave model network," in *Proc. Int. Symp. Antennas Propag.*, 2011, pp. 26–28.
- [55] U. A. Korai, L. Luini, R. Nebuloni, and I. Glesk, "Statistics of attenuation due to rain affecting hybrid FSO/RF link: Application for 5G networks," in *Proc. 11th Eur. Conf. Antennas Propag. (EuCAP)*, Mar. 2017, pp. 1789–1792.
- [56] O. Veyrunes, P. Le Clerc, and H. Sizun, "First results of precipitation effects at 30, 50, 60 and 94 GHz on a 800 m link in Belfort (France)," in *Proc. IEE Nat. Conf. Antennas Propag.*, 1999, pp. 77–80.
- [57] M. Coldrey, A. Allasia, L. Bao, E. Boch, G. Ferrari, D. Gentina, J. Putkonen, A. Sutton, L. Yigal, and N. Zein, "Maturity and field proven experience of millimetre wave transmission," Eur. Telecommun. Standards Inst., Sophia Antipolis Cedex, France, ETSI White Paper, 2015.
- [58] M. Kyro, V. Kolmonen, and P. Vainikainen, "Experimental propagation channel characterization of mm-wave radio links in urban scenarios," *IEEE Antennas Wireless Propag. Lett.*, vol. 11, pp. 865–868, 2012.
- [59] J. G. Andrews, T. Bai, M. N. Kulkarni, A. Alkhateeb, A. K. Gupta, and R. W. Heath, Jr., "Modeling and analyzing millimeter wave cellular systems," *IEEE Trans. Commun.*, vol. 65, no. 1, pp. 403–430, Jan. 2017.

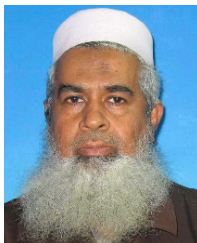


**ASMA ALI BUDALAL** received the B.Sc. degree in electrical and electronics engineering from the Faculty of Engineering, University of Benghazi, Libya, in 1999, the M.Sc. degree in electrical and computer engineering (telecommunications) from the International Islamic University Malaysia (IIUM), and the Ph.D. degree in electrical engineering and the Doctor of Philosophy degree in the field of electronic and computer engineering, specifically in wireless communication systems

from the Department of Electronic and Computer Engineering, Faculty of Engineering from IIUM. She is currently working as a Communication Engineering Lab Coordinator with the College of Electrical and Electronics Technology–Benghazi, Libya. She has published several scientific research journals and conference papers. Her current research interests include RF propagation, millimetre-wave propagation for 5G and beyond, wireless channel conditions and modelling, radio link design, RF propagation measurement, and the link level and system-level key performance indicators.



**IBRAHEEM SHAYEA** received the bachelor's degree in electronics and communication engineering from the Faculty of Engineering, University of Diyala, in July 2004, and the master's degree in communication and computer engineering and the Ph.D. degree in the field of electrical and electronic engineering, specifically in wireless communication systems from the Department of Electrical and Electronic Engineering, Faculty of Engineering and Built Environment, Universiti Kebangsaan Malaysia (UKM), Malaysia, in July 2010 and December 2015, respectively. From January 2005 to June 2006, he worked in Yemen as a computer and electronic maintenance engineer. From July 2006 to February 2007, he worked as the Maintenance Manager of the company of Computer and Research Center (CRC), Yemen. From January 2011 to December 2015 (during his Ph.D. study), he worked as a Research Assistant and a Demonstrator at the Department of Electrical and Electronic Engineering, Faculty of Engineering and Built Environment, UKM. From January 2016 to June 2018, he worked as a Postdoctoral Fellow at the Wireless Communication Center (WCC), University of Technology Malaysia (UTM), Malaysia. He had worked as a Researcher Fellow at Istanbul Technical University (ITU), Istanbul, Turkey, from September 2018 to August 2019. He has been working as an Associate Researcher with the Department of Electronics and Communications Engineering, Faculty of Electrical and Electronics Engineering, ITU, since September 2019. He is teaching courses for master's and bachelor's students. He is running research projects with Postdoctoral Researchers, and Ph.D. and master's students. He has published several scientific research journals and conference papers, and whitepapers. His research interests include mobility management in future heterogeneous (4G, 5G, and 6G) networks, mobile edge computing, machine, and deep learning, the Internet of Things (IoT), propagation of millimetre-wave, mobile broadband technology, and future data traffic growth and spectrum gap analysis.



**MD. RAFIQUK ISLAM** (Senior Member, IEEE) received the B.Sc. degree in electrical and electronic engineering from the Bangladesh University of Engineering and Technology, Dhaka, and the master's and Ph.D. degrees in electrical engineering and the Doctor of Philosophy degree from Universiti Teknologi Malaysia (UTM). He is currently a Professor with the Faculty of Electrical Engineering, International Islamic University Malaysia (IIUM). He also has a good teaching experience in the area of mobile radio communication, and wireless communication system and antennas. He was the leader for several research projects and he also involved in various research projects in wireless communication. He has published several review and research papers in national/international journals and conferences. His research interests include radio link design, RF propagation measurement and RF design, and smart antennas and array antennas design.



**MARWAN HADRI AZMI** received the B.Eng. degree (Hons.) in electrical and telecommunications from Universiti Teknologi Malaysia, in 2003, the M.Sc. degree in communications and signal processing from the Imperial College of Science, Technology and Medicine, University of London, in 2005, and the Ph.D. degree from the University of New South Wales, Australia, in 2012. He is currently a Senior Lecturer at the Wireless Communication Centre, Universiti Teknologi Malaysia. From 2012 to 2014, he spent his Sabbatical leave of absence at McGill University, Canada, working in the funded project by RIM Inc. and NSERC entitled "Cooperative Spectrum Sensing and Information Relaying in Cognitive Wireless Communications." His research interests include mobile and wireless communications, communication theory, error control coding, relay networks, spectrum sensing for cognitive radio, and iterative receiver.



**HAFIZAL MOHAMAD** (Senior Member, IEEE) received the B.Eng. (Hons.) and Ph.D. degrees in electronic engineering from the University of Southampton, U.K., in 1998 and 2003, respectively. He is currently a Professor at the Faculty of Engineering and Built Environment, Universiti Sains Islam Malaysia. He is the co-inventor of 36 filed patents and nine granted patents in the field of wireless communication. He has co-authored over 100 research papers. His research interests include wireless communication, cognitive radio, mesh networks, and the Internet of Things. He is a Registered Professional Engineer with the Board of Engineers Malaysia. He was a recipient of several awards, including the ASEAN Outstanding Scientist and Technologist Award (AOSTA) and Top Research Scientist Malaysia (TRSM) by the Academy of Sciences Malaysia. He has served in various leadership roles in the IEEE, including the Vice Chair for the IEEE Malaysia Section, in 2013, and the Chair for IEEE ComSoc/VT Chapter, from 2009 to 2011. He was the Conference Operation Chair for the IEEE ICC 2016, and the Technical Program Chair for the IEEE VTC Spring 2019 and APCC 2011. He is an enthusiastic supporter of industrial and academic liaison. He is also appointed as an expert panel for various technical committees.



**SAWSAN ALI SAAD** received the B.Sc. degree in electrical engineering from the University of Khartoum, Sudan, in 2003, and the M.Sc. and Ph.D. degrees in electrical, electronic and systems engineering from Universiti Kebangsaan Malaysia (UKM), Malaysia, in 2008 and 2016, respectively. She has worked as an Assistant Professor with The Future University, Sudan. She currently works as the Head of the Department of Computer Engineering, University of Ha'il, Saudi Arabia. Her research interests include heterogeneous networks, mobile wireless communication systems, mobility management, and the Internet of Things (IoT).



**YUSEF IBRAHIM DARADKEH** received the Doctor of Engineering Sciences degree in computer engineering and information technology (computer systems engineering and computer software engineering) from the Department of Computer Engineering and Networks, College of Engineering, Prince Sattam Bin Abdulaziz University, Saudi Arabia. He was certified as a Professional Engineer (P.Eng.). He is currently an Associate Professor with the Department of Computer Engineering and Networks, College of Engineering, Prince Sattam Bin Abdulaziz University. He is also a Senior Scientific Researcher and the Assistant Dean for Administrative Affairs. He is a dynamic academician having more than 15 years of experience specializing in teaching and scientific research development and administration experience. He has taught wide spectrum of computer science, computer engineering and networks, computer software engineering courses in undergraduate and graduate. He has been working as a Postdoctoral Research Fellow with the Department of Electrical and Computer Engineering, University of Calgary, Canada. He is a well-known and respected scientist internationally. He has an excellent experience in designing courses that bridge the gap between academia and industry as well as follow the accreditation requirements. He has published over 90 high quality refereed research papers in the international journal and conference. He has also published two books, one chapter, and an edited book in the most prestigious publications. He has Membership of the International Academy of Science and Engineering for Development (IASSED). The international recognition of his scientific achievements is demonstrated by numerous invitations to participate in the program committees of international conferences and foreign journals, as well as lecturing at renowned scientific centers around the world.

...